Journal of Hazardous Materials 178 (2010) 560–565

Contents lists available at ScienceDirect

Journal of Hazardous Materials

journal homepage: www.elsevier.com/locate/jhazmat

Template-free sol–gel preparation and characterization of free-standing visible light responsive C,N-modified porous monolithic TiO_2

Chao Chen[a,b], Weimin Cai[a,b,c,*], Mingce Long[c,**], Jingyi Zhang[c], Baoxue Zhou[a,c], Yahui Wu[a,b], Deyong Wu[c]

[a] Department of Environmental Science and Engineering, School of Municipal and Environmental Engineering, Harbin Institute of Technology, Harbin 150090, China
[b] State Key Laboratory of Urban Water Resource and Environment, Harbin Institute of Technology, Harbin 150090, China
[c] School of Environmental Science and Engineering, Shanghai Jiao Tong University, Dong Chuan Road 800, Shanghai 200240, China

ARTICLE INFO

Article history:
Received 21 September 2009
Received in revised form
18 December 2009
Accepted 25 January 2010
Available online 1 February 2010

Keywords:
Porous monolith
Titanium dioxide
Modification
Visible light
Photocatalysis

ABSTRACT

Visible light responsive C,N-modified porous monolithic titania (MT_f) has been successfully synthesized. The template-free sol–gel synthesis method accompanied by phase separation and in situ C,N-modification has been used. The molar ratio of water to tetrabutyl titanate (f) in starting solution plays an important role in the porous structure and photoactivity of MT_f. Scanning electron microscopy (SEM) analysis and N_2 adsorption–desorption analysis show that MT_f possess mesoporous structure as well as macroporous structure. MT_{22} has been further characterized by using X-ray powder diffraction (XRD), X-ray photoelectron spectroscopy (XPS), and UV–vis diffuse reflectance spectra (DRS). The results show that both nitrogen and carbon elements exist in MT_{22} and result in the visible light photocatalytic activity of MT_{22}. The observed reaction rate of decolorization of methyl orange is 0.0026 min^{-1}.

1. Introduction

Titanium dioxide is currently the most popular semiconductor in the field of clean hydrogen energy generation and recalcitrant organic pollutant degradation [1–4]. This is due to its effectiveness, cheapness and chemical stability [5,6]. However, some work should be done in the following two aspects before widespread adoption of TiO_2. The first aspect is to narrow the band gap of TiO_2, which is so wide that it can only be activated by UV light (about 3–5% of solar light). Some strategies such as metal doping [7,8] nonmetal doping [9–11], transition metal compound or dye sensitizing [12–14], have been used to extend the optical response into the visible region. The second aspect is to synthesize TiO_2 with large-dimension shape. Most of research efforts have focused on nanostructure TiO_2 powders [15–17]. However, in most cases, it is difficult to recover the powders during application, which causes the catalyst loss. Therefore, the strategy of immobilizing TiO_2 powder on the substrates with large-dimension shapes, such as film [18,19], fiber [20] and fabrics [21] has been used. Oxidizing titanium plate via anodic or peroxide to obtain nanotube or nanowire TiO_2 film [22–24] is another important method. However, generally substrate would decrease the mass transfer efficiency, therefore free-standing porous TiO_2 with shapes in large length scale is a favorable alternative. The synthesis of porous monolithic TiO_2 [25,26] has been reported and attracted increasing attention. The monolithic shape makes it easy to separate and recover TiO_2 during application and the porous structure could facilitate the mass transfer during reaction.

Sol–gel method is usually used for the synthesis of metal oxide monolith [27,28]. And only several reports about synthesis of monolithic TiO_2 through sol–gel method have been presented [26,29]. It is because that the high reactivity of titanium alkoxides makes it hard to control structure development during hydrolysis and condensation [25]. Capillary pressure formed during drying treatment makes it hard to synthesize intact monolith [30]. Although supercritical drying [30–32] and controlled solvent evaporation [33,34] are used to weaken the effect of capillary pressure, the respective rigorous condition requirement and long time requirement (longer than 30 days) make these techniques not convenient. To the best of our knowledge, only Konishi et al. [25,35] and Backlund et al. [36] have synthesized intact monoliths via drying under atmosphere and in vacuum within 7 days, respectively. Here, we report the synthesis of visible light responsive C,N-modified

* Corresponding author at: Department of Environmental Science and Engineering, School of Municipal and Environmental Engineering, Harbin Institute of Technology, Harbin 150090, China.
Tel.: +86 21 54748019; fax: +86 21 54748019.
** Corresponding author. Tel.: +86 21 54747354; fax: +86 21 54740825.
E-mail addresses: wmcai@sjtu.edu.cn (W. Cai), long_mc@sjtu.edu.cn (M. Long).

0304-3894/$ – see front matter © 2010 Elsevier B.V. All rights reserved.
doi:10.1016/j.jhazmat.2010.01.121

porous monolithic TiO_2 through sol–gel route accompanied by phase separation and in situ C,N modification. The starting solution composition was optimized, the monolith was characterized and its photocatalytic performance was studied.

2. Experimental

2.1. Sample preparation

Visible light responsive C,N-modified monolithic TiO_2 was synthesized via sol–gel method accompanied by phase separation and in situ C,N modification. In a typical procedure, 4.5 mL of acetylacetone was added in 15 mL of tetrabutyl titanate ($Ti(OBu)_4$) under modest stir and the mixture was named A solution. Another solution named B solution composed of 1.86 mL of concentrated HCl, 0.87 mL of formamide and x mL of water was made. The amount of water used in B solution depends on the molar ratio of water to tetrabutyl titanate (f). Both A solution and B solution were prepared in ice bath. B solution was added dropwise into A solution under modest stir in ice bath. The resulted solution was stirred for 5 min and then poured into tubes and allowed to gel at 30 °C. Then the gel was aged at 30 °C for 24 h and dried in oven at 60 °C for 7 days. And the dried gels were calcined at 350 °C for 1 h in air. The obtained monolithic TiO_2 prepared with different molar ratios of water to tetrabutyl titanate is named MT_f.

2.2. Characterization

The morphology of the sample was observed by a FEI SIRION 200 field emission scanning electron microscope (FESEM) (FEI). The specific surface area and pore size distribution were measured using a Nova 100 (Quantachrome Instruments) with nitrogen as the adsorption gas. The following characterizations were used for the powders of monolithic TiO_2. X-ray diffraction (XRD) analysis was performed on a Rigaku D/Max-2200/PC X-ray diffractometer. X-ray photoelectron spectroscopy (XPS) measurements were carried out on a RBD upgraded PHI-5000C ESCA system (PerkinElmer). UV–vis diffuse reflectance spectra (DRS) were recorded on a TU-1901 UV/vis spectrophotometer (Beijing Purkinje General Instrument Co., Ltd., China) and converted from reflection to absorption by the Kubelka-Munk method. Fourier transform infrared spectroscopy (FTIR) was recorded on an IR Prestige-21 system (Shimadzu Corporation, Japan). The carbon and nitrogen element contents were studied by a Vario EL III elemental analyser (Elementar, Germany).

2.3. Photocatalytic activity

Three kinds of systems are used for the photoactivity evaluation. In the first kind of test system, optical system is composed of a 1000 W xenon lamp and a cutoff filter ($\lambda > 400$ nm). MT_f was ground into powder. In a typical test, 0.05 g of catalyst powder was added into 50 mL of methyl orange solution (12 mg/L) to get a suspension, then the suspension was treated with ultrasonic for 5 min. Subsequently the light was switched on, and samples were taken, separated and analyzed at regular time intervals. The experiment without irradiation was also conducted in order to test the adsorption performance of MT_f powders. In the second kind of test system, the same optical system was used. Acetone was filled into a 20 mL reaction tube containing 0.142 g of intact MT_f to make the concentration of acetone in the tube 1 mg/L. The reaction tube was put in the dark for 1 h. The sample was taken and analyzed after 1 h irradiation by light perpendicular to the axis of reaction tube. In the third kind of test system, optical system is composed of a 300 W xenon lamp and a cutoff filter ($\lambda > 400$ nm). In a typical test, 0.061 g of intact MT_f was added into 10 mL of 12 mg/L methyl orange solution. Air is used to stir the solution. The solution with catalyst was stirred in dark for 15 min. Then the light was switched on, and the sample was taken and analyzed. The concentration of methyl orange and acetone were monitored with UNICO UV-2101 spectrometer at 464 nm and GC-2010 (Shimadzu Corporation) with a flame ionization detector, respectively.

3. Results and discussion

3.1. Morphology and photoactivity of MT_f

3.1.1. Morphology and element analysis of MT_f

The starting compositions with molar ratio f ranging from 12 to 30 have been used to synthesize MT_f. And it is found that MT_f prepared with f around 22 shows no cracks and possesses relative strong mechanical strength. SEM images of MT_f prepared with f = 21, 22, and 23 are shown in Fig. 1. The inset graph of Fig. 1b is the digital picture of MT_{22}. And the SEM images with higher magnification clearly show the existence of disorder macropores. The carbon and nitrogen contents were analyzed by elemental analysis. The results are shown in Table 1. The nitrogen contents of MT_{21} and MT_{22} are almost the same and lower than that of MT_{23}, and the carbon contents of MT_f increase in the order $MT_{22} < MT_{21} < MT_{23}$.

The successful synthesis of porous monolith in this study might be due to the starting solution composition. Acetylacetone is employed as the chelating agent to control the hydrolysis and condensation rate of titanium alkoxides [37]. HCl is used to generate strong acidity of solution, under which acetylacetone ligand of chelate complex could be protonated and then dissociated. This reaction could enhance hydrolysis and polycondensation of chelate complex forming edge-sharing chains and 3D structures [37]. Formamide is used to control pH value and phase separation during synthesis of MT_f. Konishi et al. [25] have reported the effect of formamide on the porous structure of as-synthesized monolith in detail. The gradual pH increase caused by formamide during reaction would accelerate the polycondensation reaction. The phase separation induced by formamide would result in the formation of macropores and mesopores. Water is also used to control the phase separation tendency and then affects the structure of obtained monolith [25].

3.1.2. BET specific surface area and pore structure of MT_f

The nitrogen adsorption–desorption isotherms are shown in the inset graph of Fig. 2. The pore size distribution is calculated from desorption branch of nitrogen isotherm by the Barrett-Joyner-Halenda (BJH) method (Fig. 2). MT_{21} and MT_{22} possess pores centering around 3.6 nm and 3.2 nm, respectively. However, MT_{23} possesses mainly two kinds of pores centering around 3.6 nm and 4.8 nm, respectively. The BET specific surface area of MT_{21}, MT_{22} and MT_{23} are 180 m^2/g, 361 m^2/g and 145 m^2/g, respectively. This result suggests the great effect of molar ratio f on the specific surface area and mesopore size distribution of MT_f. Combining the nitrogen adsorption–desorption analysis and SEM analysis, it can be seen that both macropores and mesopores exist in the MT_f.

3.1.3. Photocatalytic activity of MT_f

The photocatalytic activities of MT_f powders and intact MT_f have been studied using methyl orange as the model pollutant. The inset graph of Fig. 3 shows that the adsorption performance of MT_f powders decreases in the order

Table 1
Carbon and nitrogen elements content of MT_f.

MT_f	MT_{21}	MT_{22}	MT_{23}
Carbon content (w%)	2.102	1.870	2.131
Nitrogen content (w%)	1.028	1.034	1.132

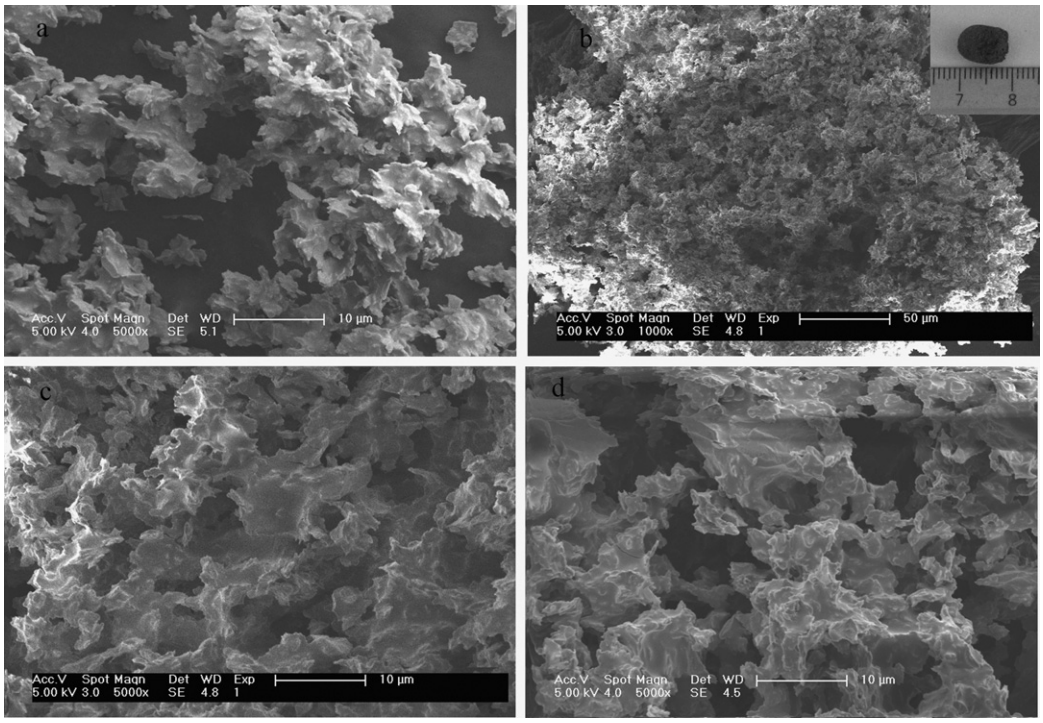

Fig. 1. SEM images of monolithic TiO_2: MT_{21} with magnification of 5000× (a); MT_{22} with magnification of 1000× (b); (inset is digital graph) and 5000× (c); MT_{23} with magnification of 5000× (d).

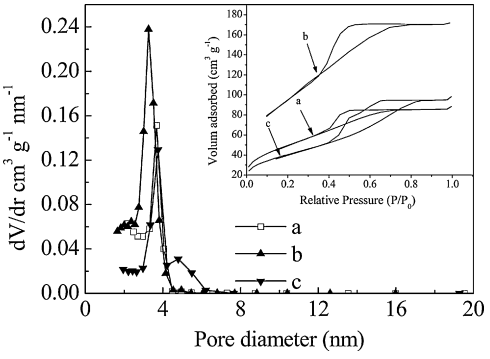

Fig. 2. BJH pore size distribution plots and N_2 adsorption–desorption isotherms (inset) of monolithic TiO_2 MT_f: (a) MT_{21}, (b) MT_{22}, and (c) MT_{23}.

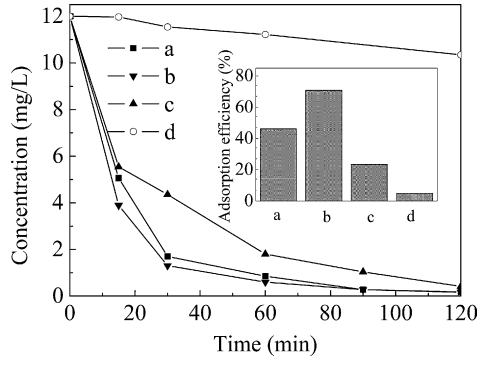

Fig. 3. Degradation of methyl orange with powders of (a) MT_{21}, (b) MT_{22}, (c) MT_{23}, and (d) P25 in the first kind of test system. Inset is adsorption of methyl orange with powders of (a) MT_{21}, (b) MT_{22}, (c) MT_{23}, and (d) P25 when the balance of adsorption and desorption is reached (1 g/L catalyst, 12 mg/L methyl orange).

MT_{22} powder > MT_{21} powder > MT_{23} powder, and the order is the same as that of specific surface area. This can be considered that the adsorption performances of MT_f powder might be affected by specific surface area and structural, crystalline properties of particles consisting MT_f. However, Fig. 4 shows a different adsorption performance of intact MT_f, which decreases in the order intact MT_{22} > intact MT_{23} > intact MT_{21}. This difference between MT_f powder and intact MT_f suggests the effect of porous structure on the adsorption performance of intact MT_f. The porous structure also plays an important role in the photocatalytic activities of MT_f. This might be approved by the different reaction rate orders of MT_f powders and intact MT_f. The photocatalytic performance of MT_f powders and intact MT_f in degradation of methyl orange decreased in the order MT_{22} powder ($0.0491\ min^{-1}$) > MT_{21} powder ($0.0440\ min^{-1}$) > MT_{23} powder ($0.0300\ min^{-1}$) (Fig. 3) and in the order intact MT_{22} ($0.0026\ min^{-1}$) > intact MT_{23} ($0.0023\ min^{-1}$) > intact MT_{21} ($0.0020\ min^{-1}$) (Fig. 4), respectively. The data in the parentheses represents the observed reaction rate

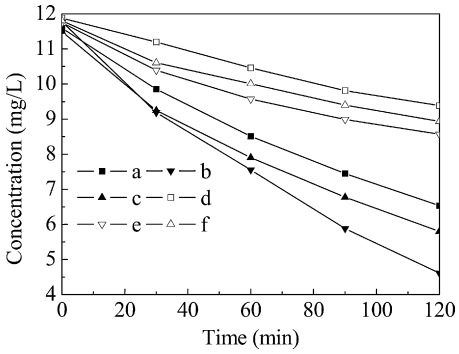

Fig. 4. Degradation of methyl orange with intact (a) MT_{21}, (b) MT_{22}, and (c) MT_{23} and adsorption of methyl orange by intact (d) MT_{21}, (e) MT_{22}, and (f) MT_{23} without irradiation in the third kind of test system (6.1 g/L catalyst, 12 mg/L methyl orange).

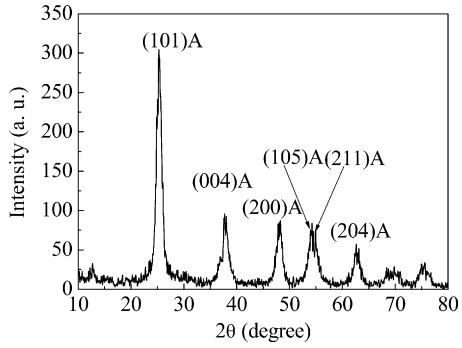

Fig. 5. XRD pattern of monolithic TiO_2 MT_{22}.

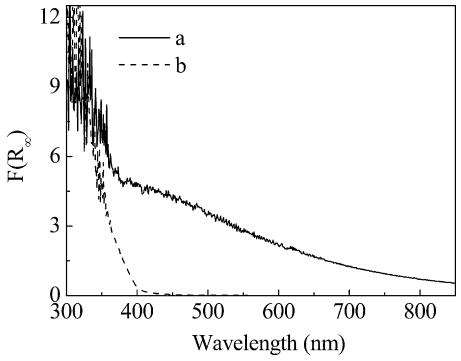

Fig. 7. UV–vis absorption spectra of (a) monolithic TiO_2 MT_{22} and (b) P25.

constant calculated based on the best linear fit to the data. A 39.9% reduction of acetone was observed during degradation of acetone with intact MT_{22} after 1 h visible light irradiation. It indicated that MT_{22} could not only degrade methyl orange but also degrade acetone. And MT_{22} has been chosen for further analysis because of its highest photocatalytic performance.

3.2. Characterization of MT_{22}

3.2.1. Phase structures

Fig. 5 shows the XRD pattern of MT_{22} powder. All diffraction peaks are indexed to pure anatase phase of TiO_2 (JPCDS Card: 84-1286). The crystallite size is calculated with Scherrer formula according to the full width at half-maximum of the (1 0 1) peak: grain size, $d = 0.9\lambda/(\beta \cos\theta)$, where 0.9 is the apparatus constant, λ is the characteristic X-ray wavelength applied (0.1545 nm) and β is the half width of the peak at the 2θ value. The average particle size is 7.8 nm.

3.2.2. FTIR study

The FTIR spectrum of MT_{22} powder is shown in Fig. 6. The spectrum is analyzed according to the Sadtler handbook database supplied by KnowItAll software if there is no specific illustration. The broad band between 3100 cm^{-1} and 3600 cm^{-1} is ascribed to the O–H stretching vibrations of surface hydroxyl groups and molecularly adsorbed water [38]. A strong band between 1550 cm^{-1} and 1680 cm^{-1} can be seen. This band could be ascribed to the H–O–H bending vibrations of the molecularly adsorbed water (around 1620 cm^{-1}) [39], N–H deformation vibration of amines (1650–1550 cm^{-1}, broad medium strong), NH_3^+ asymmetric deformation vibration (1625–1560 cm^{-1}) and N=O stretching vibration (1621–1539 cm^{-1}). The existence of N=O bond could be excluded according to the following XPS study. And the absence of N–H deformation vibration out of plane (900–650 cm^{-1}, broad strong) and NH_3^+ stretching (3200–2800 cm^{-1}, broad strong) suggest that amines and amine salts do not exist in MT_{22}. Therefore the band is inferred to be the H–O–H bending vibrations of the molecularly adsorbed water.

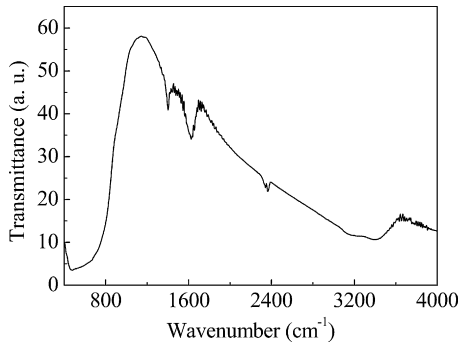

Fig. 6. FTIR spectrum for monolithic TiO_2 MT_{22}.

3.2.3. UV–vis diffuse reflectance spectra

UV–vis diffuse reflectance spectrum of MT_{22} powder is recorded using $BaSO_4$ as a reference (Fig. 7). Then the reflectance spectrum is converted into equivalent absorption spectrum by using Kubelka-Munk function ($F(R_\infty)$) [40]: $F(R_\infty) = (1 - R_\infty)^2/2R_\infty = \alpha$ (absorption coefficient)/S (scattering coefficient), where $R_\infty = R_{sample}/R_{BaSO_4}$, R_{sample} is the reflectance measurements of MT_{22} powder and P25 and R_{BaSO_4} is the reflectance measurement of $BaSO_4$.

MT_{22} shows strong absorbance in visible light region as well as ultraviolet light region and P25 shows negligible absorbance in visible light region. The indirect band-gap energy of MT_{22} is estimated according to the intercept of the tangent in the plot of $(F(R_\infty)h\nu)^{1/2}$ versus photon energy ($h\nu$). The band-gap energy is 2.78 eV with the threshold wavelength about 446 nm, which is much narrower than that of P25 (about 3.2 eV) [41]. This indicates that the as-prepared MT_{22} can be excited by the visible light, which has been proved by the decolorization of methyl orange and degradation of acetone (Section 3.1.3). The long tail in the region with wavelength larger than 446 nm is also observed, indicating the presence of surface modified species.

3.2.4. XPS studies

Fig. 8 shows the XPS spectra of MT_{22} powder. The high resolution core-level spectra of these elements were recorded to further investigate chemical states of these elements. The binding energies were all calibrated by using the contaminant carbon at binding energy of 284.6 eV. The XPS spectra of Ti2p and O1s are shown in Fig. 8a and b. The peaks at 458.3 eV and 463.8 eV are ascribed to the Ti2p3/2 and Ti2p1/2 of TiO_2 [42]. The peaks at 529.5 eV and 531.0 eV are attributed to the bulk O_2 from TiO_2 and –OH adsorbed on the surface of MT_{22}, respectively [42].

The high resolution C1s core-level XPS spectrum is shown in Fig. 8c. It can be seen that there are two peaks at 284.6 eV and 287.3 eV. The peak at 284.6 could be attributed to the adventitious carbon contamination and the peak at 287.3 eV can be assigned to the C–O bond [43]. This could be either from the carbon in the TiO_2 lattice or on the surface of TiO_2.

Fig. 8d shows the high resolution N1s core-level XPS spectrum, which could be deconvoluted into three peaks (396.1 eV, 398.7 eV and 399.7 eV). The peak at 396.1 eV could be ascribed to the substitutional nitrogen for oxygen atom [44,45]. Although the peak at 398.7 eV could be assigned to NH_3 [46], considering the results of FTIR study, we tentatively ascribe this peak to the O–Ti–N linkage [47]. Peak at 399.7 eV can be attributed to the chemisorbed N_2 molecules on MT_{22} [45,48].

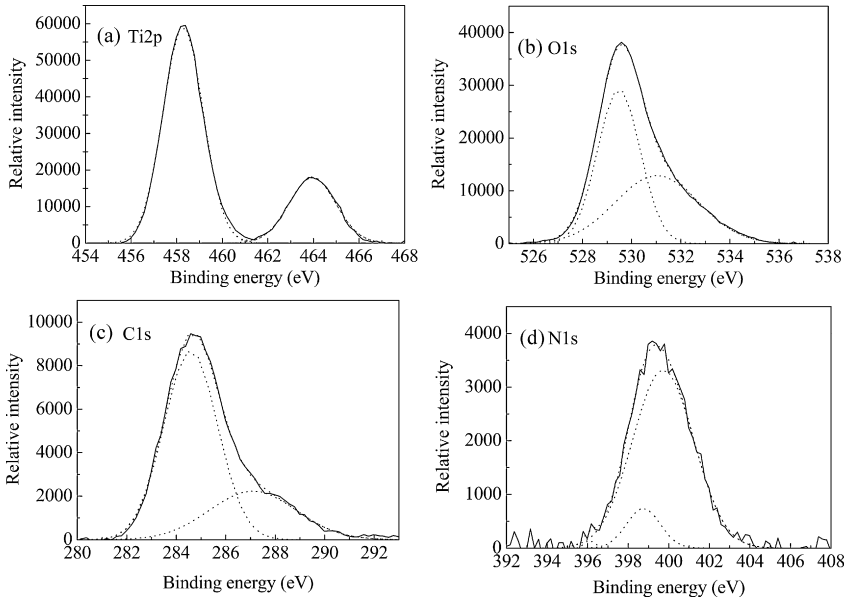

Fig. 8. XPS spectra for monolithic TiO_2 MT_{22}: (a) Ti2p, (b) O1s, (c) C1s, and (d) N1s.

Based on the above analysis, it is inferred that substitutional nitrogen for oxygen exists in the TiO_2 lattice of MT_{22}, and accounts for the band gap narrowing of TiO_2. It is hard to make clear whether the interstitial carbon and nitrogen exist in the TiO_2 lattice. However, we can infer that some compounds containing nitrogen or carbon form on the TiO_2 surface and induce the long absorption tail in UV–vis spectrum [49]. Moreover, according to the result on photocatalytic activity tests, the photocatalytic and adsorption performance of MT_{22} powders are much larger than the intact MT_{22}, although the former dosage is even lower. It can be understood that exposing inside surfaces and pores after ground into powders, the effect of water surface tension inhibiting mass transfer of methyl orange toward catalyst surface can be overcome. And in a dynamic reaction system for water purification, the porous monolithic TiO_2 is expected to be more applicable.

4. Conclusion

Visible light responsive C,N-modified TiO_2 monolith was successfully synthesized via template-free sol–gel method. This method is simple and cost effective. Considering the effect of acetylacetone used in this study on controlling the hydrolysis and polycondensation rate of tetrabutyl titanate, it is possible to synthesize TiO_2 monolith by use of other kinds of titanium alkoxides. The visible light photoactivity of as-synthesized TiO_2 monolith facilitated the application of TiO_2 monolith in a wider scope.

Acknowledgements

This work is financially supported by the National Natural Science Foundation of China (No. 20907031) and by Sate Key Laboratory of Urban Water Resource and Environment, Harbin Institute of Technology (No. QAK200805). The authors are grateful to Wei Li of the Instrumental Analysis Center of Shanghai Jiao Tong University for SEM measurements and Wenfeng Shangguan of School of Environmental Science and Engineering, Shanghai Jiao Tong University for DRS and BET analysis.

References

[1] K. Maeda, K. Teramura, D. Lu, T. Takata, N. Saito, Y. Inoue, K. Domen, Photocatalyst releasing hydrogen from water, Nature 440 (2006) 295.
[2] P.V. Kamat, Meeting the clean energy demand: nanostructure architectures for solar energy conversion, J. Phys. Chem. C 111 (2007) 2834–2860.
[3] Z.Y. Liu, X.T. Zhang, S. Nishimoto, T. Murakami, A. Fujishima, Efficient photocatalytic degradation of gaseous acetaldehyde by highly ordered TiO_2 nanotube arrays, Environ. Sci. Technol. 42 (2008) 8547–8551.
[4] M. Sleiman, C. Ferronato, J.M. Chovelon, Photocatalytic removal of pesticide dichlorvos from indoor air: a study of reaction parameters, intermediates and mineralization, Environ. Sci. Technol. 42 (2008) 3018–3024.
[5] A.L. Linsebigler, G. Lu, J.T. Yates, Photocatalysis on TiO_2 surfaces: principles, mechanisms, and selected results, Chem. Rev. 95 (1995) 735–758.
[6] X. Chen, S.S. Mao, Titanium dioxide nanomaterials: synthesis, properties, modifications, and applications, Chem. Rev. 107 (2007) 2891–2959.
[7] M.I. Litter, Heterogeneous photocatalysis: transition metal ions in photocatalytic systems, Appl. Catal. B: Environ. 23 (1999) 89–114.
[8] Z.Y. Wang, C. Chen, F.Q. Wu, B. Zou, M. Zhao, J.X. Wang, C.H. Feng, Photodegradation of rhodamine B under visible light by bimetal codoped TiO_2 nanocrystals, J. Hazard. Mater. 164 (2009) 615–620.
[9] R. Asahi, T. Morikawa, T. Ohwaki, K. Aoki, Y. Taga, Visible-light photocatalysis in nitrogen-doped titanium oxides, Science 293 (2001) 269–271.
[10] W. Zhao, W.H. Ma, C.C. Chen, J.C. Zhao, Z.G. Shuai, Efficient degradation of toxic organic pollutants with $Ni_2O_3/TiO_{2-x}B_x$ under visible irradiation, J. Am. Chem. Soc. 126 (2004) 4782–4783.
[11] C. Chen, M.C. Long, H. Zeng, W.M. Cai, B.X. Zhou, J.Y. Zhang, Y.H. Wu, D.W. Ding, D.Y. Wu, Preparation, characterization and visible light activity of carbon modified TiO_2 with two kinds of carbonaceous species, J. Mol. Catal. A: Chem. 314 (2009) 35–41.
[12] W. Zhao, C.C. Chen, W.H. Ma, J.C. Zhao, D.X. Wang, H. Hidaka, N. Serpone, Efficient photoinduced conversion of an azo dye on hexachloroplatinate(IV)-modified TiO_2 surfaces under visible light irradiation—a photosensitization pathway, Chem. Eur. J. 9 (2003) 3292–3299.
[13] Y. Cho, W. Choi, C.-H. Lee, T. Hyeon, H.-I. Lee, Visible light-induced degradation of carbon tetrachloride on dye-sensitized TiO_2, Environ. Sci. Technol. 35 (2001) 966–970.
[14] G.M. Liu, T.X. Wu, J.C. Zhao, H. Hidaka, N. Serpone, Photoassisted degradation of dye pollutants. 8. Irreversible degradation of alizarin red under visible light radiation in air-equilibrated aqueous TiO_2 dispersions, Environ. Sci. Technol. 33 (1999) 2081–2087.
[15] D. Reyes-Coronado, G. Rodriguez-Gattorno, M.E. Espinosa-Pesqueira, C. Cab, R. de Coss, G. Oskam, Phase-pure TiO_2 nanoparticles: anatase, brookite and rutile, Nanotechnology 19 (2008) 145605.
[16] P. Raveendran, M. Eswaramoorthy, U. Bindu, M. Chatterjee, Y. Hakuta, H. Kawanami, F. Mizukami, Template-free formation of meso-structured anatase TiO_2 with spherical morphology, J. Phys. Chem. C 112 (2008) 20007–20011.
[17] D.V. Bavykin, V.N. Parmon, A.A. Lapkin, F.C. Walsh, The effect of hydrothermal conditions on the mesoporous structure of TiO_2 nanotubes, J. Mater. Chem. 14 (2004) 3370–3377.
[18] Y.F. Zhu, L. Zhang, W.Q. Yao, L.L. Cao, The chemical states and properties of doped TiO_2 film photocatalyst prepared using the Sol–Gel method with $TiCl_4$ as a precursor, Appl. Surf. Sci. 158 (2000) 32–37.
[19] M. Zukalová, A. Zukal, L. Kavan, M.K. Nazeeruddin, P. Liska, M. Grätzel, Organized mesoporous TiO_2 films exhibiting greatly enhanced performance in dye-sensitized solar cells, Nano Lett. 5 (2005) 1789–1792.
[20] K. Esquivel, L.G. Arriaga, F.J. Rodríguez, L. Martínez, L.A. Godínez, Development of a TiO_2 modified optical fiber electrode and its incorporation into a

photoelectrochemical reactor for wastewater treatment, Water Res. 43 (2009) 3593–3603.
[21] D.Y. Wu, M.C. Long, J.Y. Zhou, W.M. Cai, X.H. Zhu, C. Chen, Y.H. Wu, Synthesis and characterization of self-cleaning cotton fabrics modified by TiO_2 through a facile approach, Surf. Coat. Technol. 203 (2009) 3728–3733.
[22] Y.H. Wu, M.C. Long, W.M. Cai, S.D. Dai, C. Chen, D.Y. Wu, J. Bai, Preparation of photocatalytic anatase nanowire films by in situ oxidation of titanium plate, Nanotechnology 20 (2009) 185703.
[23] Z.B. Wu, S. Guo, H.Q. Wang, Y. Liu, Synthesis of immobilized TiO_2 nanowires by anodic oxidation and their gas phase photocatalytic properties, Electrochem. Commun. 11 (2009) 1692–1695.
[24] S. Guo, Z.B. Wu, H.Q. Wang, F. Dong, Synthesis of mesoporous TiO_2 nanorods via a mild template-free sonochemical route and their photocatalytic performances, Catal. Commun. 10 (2009) 1766–1770.
[25] J. Konishi, K. Fujita, K. Nakanishi, K. Hirao, Monolithic TiO_2 with controlled multiscale porosity via a template-free sol–gel process accompanied by phase separation, Chem. Mater. 18 (2006) 6069–6074.
[26] S.O. Kucheyev, T.F. Baumann, Y.M. Wang, T. van Buuren, J.H. Satcher, Synthesis and electronic structure of low-density monoliths of nanoporous nanocrystalline anatase TiO_2, J. Electron Spectrosc. Relat. Phenom. 144 (2005) 609–612.
[27] A.E. Gash, T.M. Tillotson, J. Joe, H. Satcher, J.F. Poco, L.W. Hrubesh, R.L. Simpson, Use of epoxides in the sol–gel synthesis of porous iron(III) oxide monoliths from Fe(III) salts, Chem. Mater. 13 (2001) 999–1007.
[28] J.-H. Smtt, S. Schunk, M. Lindn, Versatile double-templating synthesis route to silica monoliths exhibiting a multimodal hierarchical porosity, Chem. Mater. 15 (2009) 2354–2361.
[29] B. Malinowska, J. Walendziewski, D. Robert, J.V. Weber, M. Stolarski, The study of photocatalytic activities of titania and titania–silica aerogels, Appl. Catal. B: Environ. 46 (2003) 441–451.
[30] A.A. Ismail, I.A. Ibrahim, Impact of supercritical drying and heat treatment on physical properties of titania/silica aerogel monolithic and its applications, Appl. Catal. A: Gen. 346 (2008) 200–205.
[31] S.O. Kucheyev, T. van Buuren, T.F. Baumann, J.H. Satcher Jr., T.M. Willey, R.W. Meulenberg, T.E. Felter, J.F. Poco, S.A. Gammon, L.J. Terminello, Electronic structure of titania aerogels from soft x-ray absorption spectroscopy, Phys. Rev. B 69 (2004) 245102.
[32] S. Cao, K.L. Yeung, P.L. Yue, An investigation of trichloroethylene photocatalytic oxidation on mesoporous titania–silica aerogel catalysts, Appl. Catal. B: Environ. 76 (2007) 64–72.
[33] L.E. Mir, A. Amlouk, E. Elaloui, M. Saadoun, A.C. Pierre, Preparation and optical characterization of transparent, microporous TiO_2 xerogel monoliths, Mater. Sci. Eng. B 146 (2008) 69–73.
[34] W.Q. Shen, F. Liu, J. Qiu, B.D. Yao, The photoinduced formation of gold nanoparticles in a mesoporous titania gel monolith, Nanotechnology 20 (2009) 105605.
[35] J. Konishi, K. Fujita, K. Nakanishi, K. Hirao, Phase-separation-induced titania monoliths with well-defined macropores and mesostructured framework from colloid-derived sol–gel systems, Chem. Mater. 18 (2006) 864–866.
[36] S. Backlund, J.-H. Smått, J.B. Rosenholm, M. Lindén, Template-free sol–gel synthesis of hierarchically macro- and mesoporous monolithic TiO_2, J. Dispers. Sci. Technol. 28 (2007) 115–119.
[37] Y.T. Kim, Y.S. Park, H. Myung, H.K. Chae, A chelate-assisted route to anatase TiO_2 nanoparticles in acidic aqueous media, Colloids Surf. A: Physicochem. Eng. Asp. 313–314 (2008) 260–263.
[38] T. Bezrodna, G. Puchkovska, V. Shimanovska, I. Chashechnikova, T. Khalyavka, J. Baran, Pyridine-TiO_2 surface interaction as a probe for surface active centers analysis, Appl. Surf. Sci. 214 (2003) 222–231.
[39] W.-C. Hung, S.-H. Fu, J.-J. Tseng, H. Chu, T.-H. Ko, Study on photocatalytic degradation of gaseous dichloromethane using pure and iron ion-doped TiO_2 prepared by the sol–gel method, Chemosphere 66 (2007) 2142–2151.
[40] D.G. Barton, M. Shtein, R.D. Wilson, S.L. Soled, E. Iglesia, Structure and electronic properties of solid acids based on tungsten oxide nanostructures, J. Phys. Chem. B 103 (1999) 630–640.
[41] J. Grzechulska, A.W. Morawski, Photocatalytic labyrinth flow reactor with immobilized P25 TiO_2 bed for removal of phenol from water, Appl. Catal. B: Environ. 46 (2003) 415–419.
[42] Y. Xie, X.J. Zhao, Y.X. Chen, Q.N. Zhao, Q.H. Yuan, Preparation and characterization of porous C-modified anatase titania films with visible light catalytic activity, J. Solid State Chem. 180 (2007) 3576–3582.
[43] S.-i. Wada, M. Takigawa, K. Matsushita, H. Kizaki, K. Tanaka, Adsorption and structure of methyl mercaptoacetate on Cu(1 1 1) surface by XPS and NEXAFS spectroscopy, Surf. Sci. 601 (2007) 3833–3837.
[44] S. Livraghi, M.R. Chierotti, E. Giamello, G. Magnacca, M.C. Paganini, G. Cappelletti, C.L. Bianchi, Nitrogen-doped titanium dioxide active in photocatalytic reactions with visible light: a multi-technique characterization of differently prepared materials, J. Phys. Chem. C 112 (2008) 17244–17252.
[45] D.M. Chen, Z.Y. Jiang, J.Q. Geng, Q. Wang, D. Yang, Carbon and nitrogen co-doped TiO_2 with enhanced visible-light photocatalytic activity, Ind. Eng. Chem. Res. 46 (2007) 2741–2746.
[46] X.B. Chen, Y.B. Lou, A.C.S. Samia, C. Burda, J.L. Cole, Formation of oxynitride as the photocatalytic enhancing site in nitrogen-doped titania nanocatalysts: comparison to a commercial nanopowder, Adv. Funct. Mater. 15 (2005) 41–49.
[47] T.C. Jagadale, S.P. Takale, R.S. Sonawane, H.M. Joshi, S.I. Patil, B.B. Kale, S.B. Ogale, N-doped TiO_2 nanoparticle based visible light photocatalyst by modified peroxide sol–gel method, J. Phys. Chem. C 112 (2008) 14595–14602.
[48] Z.P. Wang, W.M. Cai, X.T. Hong, X.L. Zhao, F. Xu, C.G. Cai, Photocatalytic degradation of phenol in aqueous nitrogen-doped TiO_2 suspensions with various light sources, Appl. Catal. B: Environ. 57 (2005) 223–231.
[49] S.-A. Gao, A.-P. Xian, L.-H. Cao, R.-C. Xie, J.-K. Shang, Influence of calcining temperature on photoresponse of TiO_2 film under nitrogen and oxygen in room temperature, Sens. Actuators B: Chem. 134 (2008) 718–726.